Novel Chiral Magnetic Domain Wall Structure in Fe/Ni/Cu(001) Films

G. Chen,[1,2] J. Zhu,[1] A. Quesada,[2] J. Li,[1] A. T. N'Diaye,[2] Y. Huo,[1] T. P. Ma,[1] Y. Chen,[1] H. Y. Kwon,[3] C. Won,[3] Z. Q. Qiu,[4] A. K. Schmid,[2,*] and Y. Z. Wu[1,†]

[1]*Department of Physics, State Key Laboratory of Surface Physics and Advanced Materials Laboratory, Center for Spintronic Devices and Applications, Fudan University, Shanghai 200433, People's Republic of China*
[2]*NCEM, Lawrence Berkeley National Laboratory, Berkeley, California 94720, USA*
[3]*Department of Physics, Kyung Hee University, Seoul 130-701, Korea*
[4]*Department of Physics, University of California at Berkeley, Berkeley, California 94720, USA*

(Received 24 January 2013; published 24 April 2013)

Using spin-polarized low energy electron microscopy, we discovered a new type of domain wall structure in perpendicularly magnetized Fe/Ni bilayers grown epitaxially on Cu(100). Specifically, we observed unexpected Néel-type walls with fixed chirality in the magnetic stripe phase. Furthermore, we find that the chirality of the domain walls is determined by the film growth order with the chirality being right handed in Fe/Ni bilayers and left handed in Ni/Fe bilayers, suggesting that the underlying mechanism is the Dzyaloshinskii-Moriya interaction at the film interfaces. Our observations may open a new route to control chiral spin structures using interfacial engineering in transition metal heterostructures.

DOI: 10.1103/PhysRevLett.110.177204 PACS numbers: 75.60.Ch, 75.70.−i

Magnetic domains and the associated domain walls (DWs) are inherent to magnetic materials and control quintessential magnetic properties, and the competition among the exchange interaction, magnetic anisotropy and the dipolar interaction governs the basic DW structures. In magnetic ultrathin films, the common textbook picture distinguishes two canonical types of DWs: Bloch walls for perpendicularly magnetized films and Néel walls for in-plane magnetized films [1,2]. While the DWs in in-plane magnetized thin films have been revealed extensively because of their greater length scale, the DWs in perpendicular magnetized thin films have not been fully explored in experiment because of their smaller size. Therefore, it remains an open question whether the Bloch wall should be necessarily the only type of DWs in perpendicularly magnetized ultrathin films although it has been the textbook example for a long time.

Furthermore, DWs involve a spin rotation in space, and one significant quantity that characterizes a DW structure is the chirality of spin rotations. Magnetic materials are usually considered to be achiral overall, and in macroscopic samples DW sections with left- and right-handed rotation sense should balance out on average. The existence of homochiral magnetic order was recently found in several materials with $B20$ crystal structure [3,4]. The chirality was attributed to the Dzyaloshinskii-Moriya interaction (DMI) [5,6] which can occur only in structures that lack inversion symmetry. In addition, homochirality was recently recognized in the cases of several ultrathin film systems [7–9], where it was attributed to nonvanishing DMI associated with absent inversion symmetry at surfaces and interfaces. Then the interesting question is whether interface-driven DMI could be strong enough to lift the left-right chiral degeneracy of DWs in thin films. Experimental tests of DW chirality in ultrathin films are important not only to the fundamental understanding of DWs and to research on topologically protected nanomagnetic structures [10], but also to the development of DW-based spintronics devices [11–13], because DW chirality has been suggested to greatly suppress the critical current density in driving DW motion [14].

In this Letter, we show that real-space imaging of the magnetic stripe phase of epitaxial Fe/Ni bilayers on Cu(001) [15,16] by spin-polarized low energy electron microscopy (SPLEEM) reveals the existence of homochiral Néel-type DWs even at room temperature. We further show that the chirality is determined by the growth order of the Fe/Ni film, supporting the inversion-symmetry breaking mechanism of the DMI at the Fe/Ni interface.

Our experiments were performed in the SPLEEM system at the National Center for Electron Microscopy at Lawrence Berkeley National Laboratory. With this instrument magnetic contrast along two in-plane axes (x and y) and along the out-of-plane direction (z) can be mapped independently with lateral resolution of the order of 10 nm [17], so that the three magnetic components $\boldsymbol{M}_x$, $\boldsymbol{M}_y$, $\boldsymbol{M}_z$ of the spin structure inside the DWs can be resolved in real space. In order to maximize the magnetic contrast, the energy of the incident electron beam was chosen to be 9.5 eV for Ni films and 9 eV for Fe films. A Cu(001) substrate with miscut angle of less than 0.1° was cleaned by cycles of Ar^+ sputtering at 1.0 keV and annealing at 600 °C. Fe and Ni layers were grown at 300 K. Film thickness was controlled by monitoring image intensity oscillations associated with atomic layer-by-layer growth. All the SPLEEM images were performed on the as-grown samples at room temperature.

Typical SPLEEM images of the out-of-plane stripe domain phase in a Fe/Ni/Cu(001) sample are shown in Figs. 1(a)–1(c). Figure 1(a) depicts the out-of-plane magnetization component $\boldsymbol{M}_z$, whereas Figs. 1(b) and 1(c) depict the in-plane magnetization components $\boldsymbol{M}_x$ and $\boldsymbol{M}_y$, respectively. The strong contrast in the $\boldsymbol{M}_z$ image indicates perpendicular magnetization of the stripe domains in this film. In the $\boldsymbol{M}_y$ image, very weak contrast on stripe domains indicates that magnetization of the stripe domains is canted towards to the in-plane direction by approximately 2°; such canting has been theoretically predicted for a stripe domain phase near spin reorientation transition [18]. In order to clearly show the direction of the magnetization vector in Fig. 1(d), the in-plane components of the magnetization in the DW are represented by color and the out-of-plane component represented by gray ($+\boldsymbol{M}_z$) and black ($-\boldsymbol{M}_z$). It is believed that, in theory, Bloch-type DW structure should be a ground state in stripe phases because the in-plane magnetization components of Néel-type DWs would add additional magnetic dipole energy [1,19]. Our domain images, however, always show a perpendicular relation between the DW in-plane magnetization and the stripe directions, which means that the DWs between the stripe domains in Fe/Ni bilayers are Néel type, as opposed to the theoretically predicted Bloch type. In addition, each DW displays only a single color [Fig. 1(d)], indicating a fixed chirality along each individual DW. Moreover, the in-plane magnetization of neighboring DWs always alternates; i.e., the in-plane moments of the DWs always point from the $+\boldsymbol{M}_z$ domain to the neighboring $-\boldsymbol{M}_z$ domain. This result shows that the stripe domain pattern is an inhomogeneous spin cycloid with right-handed chiral DWs [Fig. 1(e)] [20]. We found that this right-handed chirality is a well-reproduced phenomenon over the sample area, and also independent of the DW orientation, indicating that the observed chiral DWs in the Fe/Ni bilayer are isotropic in the film plane.

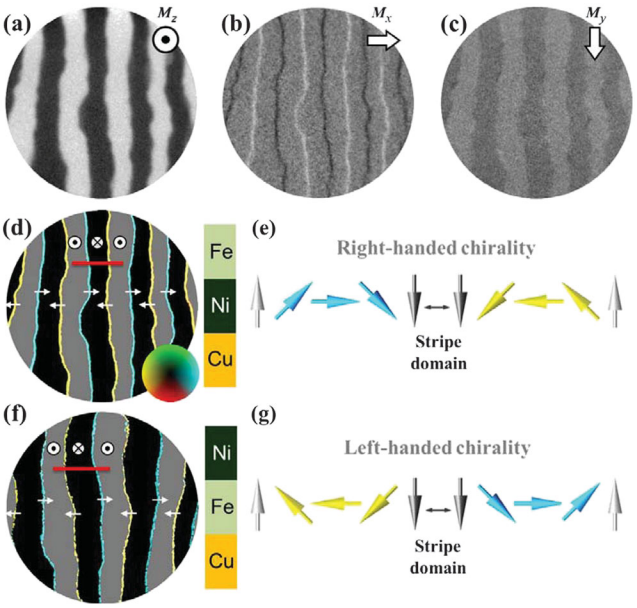

FIG. 1 (color). (a)–(c) SPLEEM images of 2.5 ML Fe/2 ML Ni/Cu(001) mapping orthogonal magnetization components: (a) $\boldsymbol{M}_z$, (b) $\boldsymbol{M}_x$, (c) $\boldsymbol{M}_y$. Top right symbols define x, y, z axis and spin directions. The field of view is 8 μm. (d) Compound image constructed from the SPLEEM images in (a)–(c) highlighting the DW. The color wheel represents the direction of in-plane magnetization. (e) Schematic of chiral DWs along the red line in (d), showing right-hand chirality [20]. (f) Compound magnetic image observed in a Ni/Fe/Cu(001) sample. (g) Schematic of chiral DWs along red line in (f), showing left-hand chirality [20]. White arrows in (d) and (f) indicate the in-plane spin orientations inside the DWs.

The presence of homochirality cannot be explained by exchange interaction, dipolar interaction, and anisotropy alone because these interactions won't lead to a chiral preference. Chirality emerges when conventional models of magnetism are augmented with the DMI [5,6]. The energy contribution from the DMI can be written as $E_{\mathrm{DM}} = \boldsymbol{D}_{ij} \cdot (\boldsymbol{S}_i \times \boldsymbol{S}_j)$, where $\boldsymbol{D}_{ij}$ is the DMI vector, $\boldsymbol{S}_i$ and $\boldsymbol{S}_j$ are magnetic spin moments located on neighboring atomic sites i and j. Hence the DMI favors magnetic spins on neighboring atomic sites to be aligned orthogonally, and the energy competition between the DMI and the exchange coupling will lead to a noncollinear spin structures with a fixed chirality.

In layered structures made of high-symmetry materials, the DMI arises from spin-orbit scattering of electrons in the inversion asymmetric crystal field at the interfaces [7–9]. For a thin film system such as Fe/Ni/Cu(001), we can apply the symmetry conditions given in Ref. [6] and deduce that $\boldsymbol{D}_{ij}$ vector lies in the film plane and perpendicularly to the spin-spiral direction; i.e., $\boldsymbol{D}_{ij}$ should be perpendicular to the position vector connecting neighboring spins. For Bloch DWs, the vector $\boldsymbol{S}_i \times \boldsymbol{S}_j$ is parallel to the spin-spiral propagation direction (e.g., perpendicular to the vector $\boldsymbol{D}_{ij}$) so that the DMI of $E_{\mathrm{DM}} = \boldsymbol{D}_{ij} \cdot (\boldsymbol{S}_i \times \boldsymbol{S}_j)$ vanishes. For Néel-type DWs, the vector $\boldsymbol{S}_i \times \boldsymbol{S}_j$ is perpendicular to the spin-spiral propagation direction so that the nonzero DMI lifts the left-right chiral degeneracy, resulting in a fixed chirality of the Néel-type DWs. Therefore a Bloch-to-Néel DW transition is expected as the DMI strength exceeds a critical value. In such a case, the ground state will no longer be Bloch DWs but Néel-type DWs with a fixed chirality determined by the sign of the DMI, as seen in the SPLEEM images shown in Fig. 1.

To further clarify how the DMI stabilizes the chiral DWs, we constructed a two-dimensional Heisenberg model that includes the exchange interaction, magnetic anisotropy, dipolar interaction, and the DMI [21] to simulate the magnetic domains by Monte Carlo simulation. Although this computer model is not designed be compared quantitatively with the experimental result, it captures the essential magnetic features in the Fe/Ni/Cu(001)

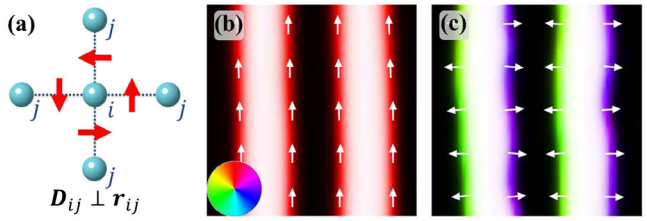

FIG. 2 (color online). (a) Schematic of the DM vector $\boldsymbol{D}_{ij}$ (red arrows) and lattice vectors $\boldsymbol{r}_{ij}$. (b) Monte Carlo simulation result of the stripe domain with $\boldsymbol{D}_{ij} = 0$ shows achiral Bloch-type DWs. (c) Simulated stripe domain with sufficiently large $\boldsymbol{D}_{ij}$ shows chiral Néel-type DWs. The color wheel shown in (b) represents the direction of in-plane magnetization. The white arrows in (b)–(c) correspond to in-plane spin orientations inside the DWs.

system. We implemented a two-dimensional square lattice with periodic boundary conditions and nonzero $\boldsymbol{D}_{ij}$ vectors for nearest neighbor sites, separated by the lattice vectors $\boldsymbol{r}_{ij}$. The Fe/Ni/Cu(001) system has an fcc crystalline structure and the $\boldsymbol{D}_{ij}$ vectors must reflect the fourfold rotational symmetry of the system, as sketched in Fig. 2(a) [22]. With zero DMI strength, this model results in a stripe domain phase which is the lowest energy state due to the competition between long range dipolar interaction and short range exchange interaction [15]. Such stripe domains contain only Bloch DWs, as expected [Fig. 2(b)]. (Metastable disorder and defects within the simulated stripe domain patterns were removed by simulating small in-plane magnetic field pulses.) To see how the DMI leads to Néel-type chiral DWs, we gradually increase the strength of DMI in the simulation. We find that the spins inside the DWs rotate from the direction parallel to the DW direction (Bloch-type) to the direction orthogonal to the DW direction (Néel-type) as the magnitude of the $\boldsymbol{D}_{ij}$ vectors exceeds a threshold value. The resulting Néel-type DWs shown in Fig. 2(c) all have fixed chirality and spins in neighboring DWs aligned antiparallel, consistent with our experimental observation. By reversing the sign of the DMI, opposite DW chirality is obtained from the simulated domains. The detailed model and parameters for our Monte Carlo simulation can be found in the Supplemental Material [23].

Several implications that follow from this model can be tested experimentally. The short-range nature of the DMI implies that the homochirality of the Néel DWs is a local property that should not depend on the distance to neighboring DWs. This can be tested by looking at a well-known feature of magnetic stripe phases [15], the exponential decrease of the stripe width with film thickness near a spin reorientation transition point: keeping the Ni film thickness fixed at 2 monolayer (ML) and increasing the Fe layer thickness by a few percent in the vicinity of 2.5 ML, we find that the stripe width decreases by orders of magnitude (10 to 0.3 μm) as the spin reorientation

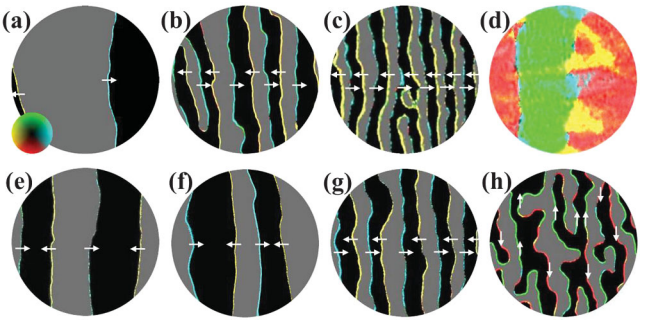

FIG. 3 (color). (a)–(d) Compound magnetic images in Fe/2 ML Ni/Cu(001) samples with Fe layer thickness d_{Fe} of (a) 2.43 ML, (b) 2.46 ML, (c) 2.50 ML, and (d) 2.51 ML. (e)–(h) Compound magnetic images in Fe/Ni/Cu(001) samples with different Ni layer thickness d_{Ni}, (e) $d_{\mathrm{Ni}} = 1$ ML, $d_{\mathrm{Fe}} = 2$ ML, (f) $d_{\mathrm{Ni}} = 2$ ML, $d_{\mathrm{Fe}} = 2.5$ ML, (g) $d_{\mathrm{Ni}} = 7$ ML, $d_{\mathrm{Fe}} = 2$ ML, (h) $d_{\mathrm{Ni}} = 10$ ML, $d_{\mathrm{Fe}} = 1.3$ ML. The field of view is 8 μm except in (c) where it is 4 μm. White arrows correspond to in-plane spin orientations inside the DWs. The color wheel shown in (a) represents the direction of in-plane magnetization.

transition is approached [Figs. 3(a)–3(d)]. Notably, these images show that Néel-type DW structure and the right-handed chirality are robust features of this system, consistent with the interpretation that the short-ranged DMI is the driving force of this DW chirality. In addition, recalling that the DMI in the Fe/Ni/Cu(001) system is an interfacial effect suggests that its contribution to the magnetic structure should decrease with increasing thickness of the structure until, above some threshold, a transition from the chiral Néel-type DWs to achiral Bloch-type DWs would be expected. This prediction was confirmed, as shown in Figs. 3(e)–3(h). By increasing mainly the Ni film thickness while keeping the Fe layer thin, the bilayer structure remains in the stripe phase over a wide thickness range [16]. We find that the Néel-type DWs with right-handed chirality persist up to 7 ML Ni thickness [Figs. 3(e) to 3(g)], and then switch to the Bloch-type above 10 ML Ni thickness [Fig. 3(h)]. These Bloch DWs are magnetized parallel to the DW plane with the in-plane magnetization component randomly distributed in sections along each single DW [as marked by arrows in Fig. 3(h)], indicating absence of magnetic homochirality in this situation. The simultaneous switching of the DWs from Néel-to-Bloch type and the loss of homochirality in thicker Ni films support the fact that the observed magnetic chirality is an interfacial effect.

The interfacial character of the DMI also suggests that the sign of the DMI could be altered by reversing the Fe and Ni film order. To test this idea we grew Ni/Fe/Cu(001) samples and found that the in-plane magnetization component in the DWs in Ni/Fe/Cu(001) always points from $-\boldsymbol{M}_z$ domain to $+\boldsymbol{M}_z$ domain [Fig. 1(f)], i.e., in the opposite direction as compared to the DWs in Fe/Ni/Cu(001). This shows that the domain structure in the Ni/Fe bilayers is now a spin cycloid with *left-handed* chirality [see Fig. 1(g)].

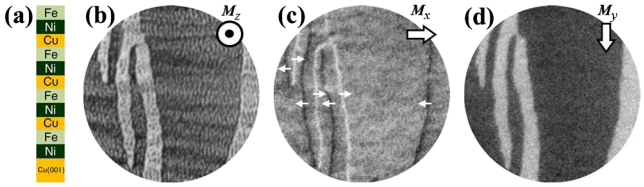

FIG. 4 (color online). (a) Schematic of stacked $[Fe/Ni/Cu]_n$ multilayer. (b)–(d) SPLEEM images with x, y, z components of $\boldsymbol{M}$ from Fe(1.5)/Ni(2)/$[Cu(2)/Fe(2.2)/Ni(2)]_2$/Cu(2)/Fe(1.2)/Ni(2)/Cu(001) (number's unit is ML). The field of view is 8 μm. White arrows in (c) correspond to in-plane spin orientations inside the DWs.

The strength of the DMI in Fe/Ni/Cu(001) system can be estimated from the experimentally observed Néel-to-Bloch DW transition thickness. Since the exchange energy and the anisotropy energy are equal for both type DW structures, the final DW type is determined by the energy competition between the DMI energy and the dipolar energy. The DMI energy is zero for Bloch walls and reduces the energy by $\sim\pi \times |\boldsymbol{D}_{ij}|$ in a Néel DW [20,23]. The dipolar energy is smaller in Bloch DWs than Néel DWs [1,19] by a quantity proportional to the total magnetization. Therefore we are able to estimate the strength of the DMI by calculating the dipolar energy difference at the Néel-to-Bloch DW transition. By calculating the Néel-wall case in Fe(2 ML)/Ni(7 ML)/Cu(001) and the Bloch-wall case in Fe(1.3 ML)/Ni(10 ML)/Cu(001), we bracket the DMI value in the Fe/Ni/Cu(001) system to be 0.12–0.17 meV per atom [23]. This estimated DMI value is about one order of magnitude smaller than that observed in the Mn/W(001) system [8]. Theoretically, the magnitude of the DMI vector is related to the spin-orbit coupling and electronic structure of the system [6]. Thus the weaker DMI in our Fe/Ni/Cu(001) system is not unexpected because the spin-orbit coupling strength in Fe, Ni, and Cu substrate is relatively weaker than that in the tungsten substrate in the Mn/W(001) system. This DMI is much smaller than the exchange coupling so that it can't induce a spin spiral structure at the atomic scale as shown in Mn/W(001) system [8]; however, it is sufficiently strong to stabilize the chiral spin structure in the DWs of the stripe phase.

We have shown that the contribution of interfacial DMI to the magnetic structure decreases with increasing layer thickness; hence, one might expect that DMI-driven chiral DWs should exist only in ultrathin films, which may limit its application in DW-based spintronics devices. This limitation can be overcome by stacked multilayers. To avoid likely cancellation of the antisymmetric DMI at Fe/Ni and Ni/Fe interfaces in $(Fe/Ni)_n$ multilayers, we prepared $(Fe/Ni/Cu)_n$ multilayers where only one type of the Fe/Ni interface exists in each period [see Fig. 4(a)]. Carefully tuning the thickness of each layer to maintain perpendicular magnetic anisotropy, we constructed $(Fe/Ni/Cu)_n$ multilayer stacks up to $n = 4$, with 21 ML total thickness of the structures. SPLEEM imaging confirms that the right-handed chiral DWs remain stable: as shown in Figs. 4(b)–4(d), the magnetization inside the DWs is always along the x direction and is always antiparallel in neighboring DWs. In this stacked system, the perpendicular anisotropy is weak and the magnetization cants $\sim 18°$ away from the surface plane so that both z and y components inside the stripe domains show clear magnetic contrast. Recalling that the transition thickness between the chiral Néel-type DW and the achiral Bloch-type DW in Fe/Ni bilayer is around 10 ML, we attribute the observed increase of the transition thickness to 21 ML in the multilayer stack to the enhancement of the effective DMI.

These real-space observations of the Néel-type chiral DW structures in Fe/Ni/Cu(001) not only prove the existence of chiral magnetic order at room temperature, but also open a new route to explore the DMI in magnetic bilayers from both experimental and theoretical points of view. By controlling the growth order of the Fe and Ni layers, we provide an effective way to change the magnetic chirality in magnetic thin films. Moreover, our results demonstrate the possibility of enhancing the DMI in stacked magnetic multilayers, which enables the development of devices made of 3d transition metals that integrate spin spirals to achieve novel spintronics functionalities.

We acknowledge helpful discussions with Professor X. F. Jin. This work was supported by MOST Grants No. 2011CB921801, No. 2009CB929203, and No. 2010DFA52220, by NSFC Grants No. 10834001, No. 10925416, and No. 11274074 of China, by WHMFC Grant No. WHMFCKF2011008, by a Grant from the National Research Foundation of Korea, funded by the Korean Government (2009-0074324), by the National Science Foundation under Grant No. DMR-1210167, and by NRF through the Global Research Laboratory project of Korea. Experiments were performed at the National Center for Electron Microscopy, Lawrence Berkeley National Laboratory, supported by the Office of Science, Office of Basic Energy Sciences, Scientific User Facilities Division, of the U.S. Department of Energy under Contract No. DE-AC02—05CH11231.

*To whom all correspondence should be addressed.
akschmid@lbl.gov
†wuyizheng@fudan.edu.cn

[1] A. Hubert and R. Schäfer, *Magnetic Domains: The Analysis of Magnetic Microstructures* (Springer, Berlin, 1998).
[2] S. Chikazumi, *Physics of Ferromagnetism* (Oxford University Press, Oxford, 1999).
[3] M. Uchida, Y. Onose, Y. Matsui, and Y. Tokura, Science **311**, 359 (2006).

[4] S. Mühlbauer, B. Binz, F. Jonietz, C. Pfleiderer, A. Rosch, A. Neubauer, R. Georgii, and P. Böni, Science **323**, 915 (2009).
[5] I. E. Dzyaloshinskii, Sov. Phys. JETP **5**, 1259 (1957).
[6] T. Moriya, Phys. Rev. **120**, 91 (1960).
[7] M. Bode, M. Heide, K. von Bergmann, P. Ferriani, S. Heinze, G. Bihlmayer, A. Kubetzka, O. Pietzsch, S. Blügel, and R. Wiesendanger, Nature (London) **447**, 190 (2007).
[8] P. Ferriani, K. von Bergmann, E. Y. Vedmedenko, S. Heinze, M. Bode, M. Heide, G. Bihlmayer, S. Blügel, and R. Wiesendanger, Phys. Rev. Lett. **101**, 027201 (2008).
[9] S. Heinze, K. von Bergmann, M. Menzel, J. Brede, A. Kubetzka, R. Wiesendanger, G. Bihlmayer, and S. Blügel, Nat. Phys. **7**, 713 (2011).
[10] R. Skomski, Z. Li, R. Zhang, R. D. Kirby, A. Enders, D. Schmidt, T. Hofmann, E. Schubert, and D. J. Sellmyer, J. Appl. Phys. **111**, 07E116 (2012).
[11] S. S. P. Parkin, M. Hayashi, and L. Thomas, Science **320**, 190 (2008).
[12] M. Hayashi, L. Thomas, R. Moriya, C. Rettner, and S. S. P. Parkin, Science **320**, 209 (2008).
[13] D. A. Allwood, G. Xiong, C. C. Faulkner, D. Atkinson, D. Petit, and R. P. Cowburn, Science **309**, 1688 (2005).
[14] O. A. Tretiakov and Ar. Abanov, Phys. Rev. Lett. **105**, 157201 (2010).
[15] Y. Z. Wu, C. Won, A. Scholl, A. Doran, H. W. Zhao, X. F. Jin, and Z. Q. Qiu, Phys. Rev. Lett. **93**, 117205 (2004).
[16] J. Choi, J. Wu, C. Won, Y. Z. Wu, A. Scholl, A. Doran, T. Owens, and Z. Q. Qiu, Phys. Rev. Lett. **98**, 207205 (2007).
[17] N. Rougemaille and A. K. Schmid, Eur. Phys. J. Appl. Phys. **50**, 20101 (2010).
[18] J. P. Whitehead, A. B. MacIsaac, and K. De'Bell, Phys. Rev. B **77**, 174415 (2008).
[19] Y. Yafet and E. M. Gyorgy, Phys. Rev. B **38**, 9145 (1988).
[20] M. Heide, G. Bihlmayer, and S. Blügel, Phys. Rev. B **78**, 140403(R) (2008).
[21] H. Y. Kwon, K. M. Bu, Y. Z. Wu, and C. Won, J. Magn. Magn. Mater. **324**, 2171 (2012).
[22] E. Y. Vedmedenko, L. Udvardi, P. Weinberger, and R. Wiesendanger, Phys. Rev. B **75**, 104431 (2007).
[23] See Supplemental Material at http://link.aps.org/supplemental/10.1103/PhysRevLett.110.177204 for Monte Carlo simulation details and an estimation of the magnitude of the DMI vector.